You might find this additional information useful...

This article cites 49 articles, 26 of which you can access free at:
http://jap.physiology.org/cgi/content/full/101/1/354#BIBL

Updated information and services including high-resolution figures, can be found at:
http://jap.physiology.org/cgi/content/full/101/1/354

Additional material and information about *Journal of Applied Physiology* can be found at:
http://www.the-aps.org/publications/jappl

This information is current as of December 12, 2006 .

HIGHLIGHTED TOPIC | *Regulation of the Cerebral Circulation*

Cerebral hemodynamics during orthostatic stress assessed by nonlinear modeling

Georgios D. Mitsis,[1] Rong Zhang,[2] Benjamin D. Levine,[2] and Vasilis Z. Marmarelis[1]

[1]*Department of Biomedical Engineering, University of Southern California, Los Angeles, California;*
and [2]*Institute for Exercise and Environmental Medicine, University of Texas Southwestern*
Medical Center at Dallas and Presbyterian Hospital of Dallas, Dallas, Texas

Mitsis, Georgios D., Rong Zhang, Benjamin D. Levine, and Vasilis Z. Marmarelis. Cerebral hemodynamics during orthostatic stress assessed by nonlinear modeling. *J Appl Physiol* 101: 354–366, 2006. First published March 2, 2006; doi:10.1152/japplphysiol.00548.2005.—The effects of orthostatic stress, induced by lower body negative pressure (LBNP), on cerebral hemodynamics were examined in a nonlinear context. Spontaneous fluctuations of beat-to-beat mean arterial blood pressure (MABP) in the finger, mean cerebral blood flow velocity (MCBFV) in the middle cerebral artery, as well as breath-by-breath end-tidal CO_2 concentration ($P_{ET_{CO_2}}$) were measured continuously in 10 healthy subjects under resting conditions and during graded LBNP to presyncope. A two-input nonlinear Laguerre-Volterra network model was employed to study the dynamic effects of MABP and $P_{ET_{CO_2}}$ changes, as well as their nonlinear interactions, on MCBFV variations in the very low (VLF; below 0.04 Hz), low (LF; 0.04–0.15 Hz), and high frequency (HF; 0.15–0.30 Hz) ranges. Dynamic cerebral autoregulation was described by the model terms corresponding to MABP, whereas cerebral vasomotor reactivity was described by the model $P_{ET_{CO_2}}$ terms. The nonlinear model terms reduced the output prediction normalized mean square error substantially (by 15–20%) and had a prominent effect in the VLF range, both under resting conditions and during LBNP. Whereas MABP fluctuations dominated in the HF range and played a significant role in the VLF and LF ranges, changes in $P_{ET_{CO_2}}$ accounted for a considerable fraction of the VLF and LF MCBFV variations, especially at high LBNP levels. The magnitude of the linear and nonlinear MABP-MCBFV Volterra kernels increased substantially above −30 mmHg LBNP in the VLF range, implying impaired dynamic autoregulation. In contrast, the magnitude of the $P_{ET_{CO_2}}$-MCBFV kernels reduced during LBNP at all frequencies, suggesting attenuated cerebral vasomotor reactivity under dynamic conditions. We speculate that these changes may reflect a progressively reduced cerebrovascular reserve to compensate for the increasingly unstable systemic circulation during orthostatic stress that could ultimately lead to cerebral hypoperfusion and syncope.

lower body negative pressure; mean cerebral blood flow velocity; Laguerre-Volterra network

ORTHOSTATIC INTOLERANCE affects individuals with pathophysiological conditions such as autonomic failure, as well as normal individuals after prolonged exposure to microgravity or bed-rest deconditioning (5). The underlying mechanisms are still not clear and likely multifactorial (26). Orthostatic intolerance may lead to the development of syncope, induced by a substantial reduction in cerebral blood flow (CBF).

Several studies have reported a marked decrease in steady-state mean cerebral blood flow velocity (MCBFV) during head-up tilt (HUT) and lower body negative pressure (LBNP), despite the maintenance of a relatively constant steady-state value of mean arterial blood pressure (MABP). These findings suggest the presence of a paradoxical cerebral vasoconstriction, which may be induced by a reduction in arterial CO_2 and/or sympathetic activation elicited by orthostatic stress (4, 16, 21, 27, 53). Moreover, a significant increase in the gain of the transfer function estimates between spontaneous beat-to-beat fluctuations of MABP and MCBFV was reported at high levels of LBNP (53), suggesting impaired dynamic cerebral autoregulation. In addition, dynamic cerebral autoregulation was found to be dependent on end-tidal CO_2 ($P_{ET_{CO_2}}$) level and impaired during HUT by analyzing transfer function estimates between fluctuations of MABP and beat-to-beat cerebrovascular resistance (12). In contrast to these observations, dynamic autoregulation was found to remain unchanged during HUT (46, 47).

Dynamic cerebral autoregulation has been studied extensively by use of MABP and MCBFV variations by both linear (3, 15, 23, 37, 52) and nonlinear (33, 38) methods. These studies have demonstrated clearly that dynamic cerebral autoregulation is a frequency-dependent phenomenon. Impulse response or transfer function estimates in linear analysis and Volterra models in nonlinear analysis have specifically shown that autoregulation is more effective below 0.1 Hz, where most of the MABP spectral power resides, i.e., most MABP changes are attenuated effectively (15, 33, 52). However, the presence of significant frequency-dependent nonlinearities, which were found to be prominent below 0.04 Hz (33), revealed the limitations of linear analysis methods in quantifying dynamic autoregulation. Moreover, because arterial CO_2 tension (Pa_{CO_2}) is one of the strongest physiological modulators of CBF (11), a number of studies have examined the dynamic effects of Pa_{CO_2} changes on MCBFV (cerebral vasomotor reactivity) by employing step CO_2 changes (14, 40), controlled breathing protocols (13), as well as spontaneous breath-by-breath $P_{ET_{CO_2}}$ fluctuations along with MABP fluctuations (34, 39). Specifically, it was shown that the effects of changes in $P_{ET_{CO_2}}$ on

MCBFV variations are time delayed, strongly nonlinear, and significant below 0.04 Hz (34).

Previous studies of dynamic autoregulation under orthostatic stress employed linear modeling methods and did not account for the effects of Pa_{CO_2}. Specifically, the effects of orthostatic stress on dynamic autoregulation of very slow MABP changes have not been quantified, owing to the inherent limitations of linear methodologies in this frequency range (47, 53). Therefore, the purpose of this study is to extend previous findings by utilizing a nonlinear, multiple-input modeling methodology to assess dynamic cerebral autoregulation and cerebral vasomotor reactivity simultaneously during graded LBNP over the entire naturally occurring frequency range of the hemodynamic signal variations. To this end, we employed a newly developed methodology termed the Laguerre-Volterra network (LVN) (31, 32) to model the dynamic effects of MABP and $P_{ET_{CO_2}}$ changes on MCFBV variations. This approach has been used successfully for modeling dynamic cerebral autoregulation and cerebral vasomotor reactivity under resting conditions in our laboratory's recent studies (33, 34).

METHODS

Experimental methods. This is a retrospective study, and the data analysis using linear transfer function has been reported previously (53). The experimental methods are described briefly herein. Ten healthy subjects (5 men) with a mean age of 32.1 ± 7.3 yr, height of 169.6 ± 11.1 cm, and weight 68.9 ± 13.9 kg voluntarily participated in the study. All were nonsmokers and were free of known cardiovascular, pulmonary, and cerebrovascular disorders. Each subject was informed of the experimental procedures, which were approved by the Institutional Review Boards of The University of Texas Southwestern Medical Center and Presbyterian Hospital of Dallas, and signed a written consent form.

Orthostatic stress was induced by graded LBNP. Subjects were placed supine in an LBNP box that was sealed at the level of the iliac crests. After at least a 30-min baseline period of quiet rest, the magnitude of the suction was increased incrementally according to the following protocol: -15 mmHg for 13 min, -30 mmHg for 13 min, and then progressively by -10 mmHg every 13 min to the point of maximal tolerance. LBNP was terminated if the subject developed signs and/or symptoms of presyncope: sudden onset of nausea, sweating, light-headedness, bradycardia, or sustained hypotension.

Heart rate (HR) was monitored by ECG, and arterial pressure was measured continuously in the finger by photoplethysmography (Finapres, Ohmeda). Cerebral blood flow velocity (CBFV) was obtained continuously in the middle cerebral artery by transcranial Doppler. A 2-MHz probe (DWL Elektronische Systeme) was placed over the subject's temporal window and fixed at a constant angle and position with an adjustable headgear to obtain optimal signals according to standard techniques (1). Breath-by-breath $P_{ET_{CO_2}}$ was also monitored continuously via a nasal cannula by using a mass spectrometer (MGA 1100, Marquette Electronics).

After a 6-min period of baseline data collection, LBNP was applied. At each LBNP level, 6 min of data were collected, after a 2-min period at the beginning for stabilization of cardiovascular hemodynamics. The intermittent arterial pressure measured in the subject's upper arm was also monitored at each level of LBNP to corroborate the corresponding recordings from the finger.

Mathematical methods and data analysis. The beat-to-beat MABP, MCBFV, and breath-by-breath $P_{ET_{CO_2}}$ data were resampled at 1 Hz to create evenly sampled time series and were then high-passed at 0.005 Hz. Steady-state values and variabilities (standard deviations around mean value) of MABP, MCBFV, and $P_{ET_{CO_2}}$ were calculated over the

6-min data segments for each subject and then group averaged at baseline and during LBNP. The power spectral density (PSD) of the signals was estimated by employing the Welch modified periodogram method (42). Their segmental spectral power (SSP) was calculated by integrating the PSD in the very low (VLF; 0.005–0.04 Hz), low (LF; 0.04–0.15 Hz), and high frequency ranges (HF; 0.15–0.30 Hz), respectively. The frequency range limits were selected on the basis of the results of the present and previous studies, which have shown that the dynamic effects of nonlinearities and CO_2 are more prominent in the VLF range (33, 34). Changes in the steady-state hemodynamics and spectral power during LBNP were compared by one-way analysis of variance and Tukey's honestly significant difference post hoc test for multiple comparisons, with the significance level set to $P < 0.05$.

The presence of significant nonlinearities in cerebral hemodynamics is well established (33, 34, 38, 52). We thus employed a novel variant of the general Volterra-Wiener approach, termed the LVN (30, 31), to obtain quantitative nonlinear models of the dynamic effects of spontaneous MABP and $P_{ET_{CO_2}}$ changes on MCBFV variations. The LVN methodology combines Laguerre function expansions (29) with Volterra networks (i.e., networks with polynomial activation functions) and has been shown to yield accurate nonlinear models from short stimulus-response records (31, 32). Recently, this approach has been used successfully to model cerebral autoregulation and cerebral vasomotor reactivity under resting conditions (33, 34). Here we employed the multiple-input LVN (MI-LVN) (32), whereby the two inputs of the model were MABP and $P_{ET_{CO_2}}$ changes and the output was MCBFV variations. An equivalent diagram is shown in Fig. 1, which illustrates that the MI-LVN consists of linear and nonlinear terms that correspond to each input, as well as cross-terms that correspond to the nonlinear interactions between the two inputs.
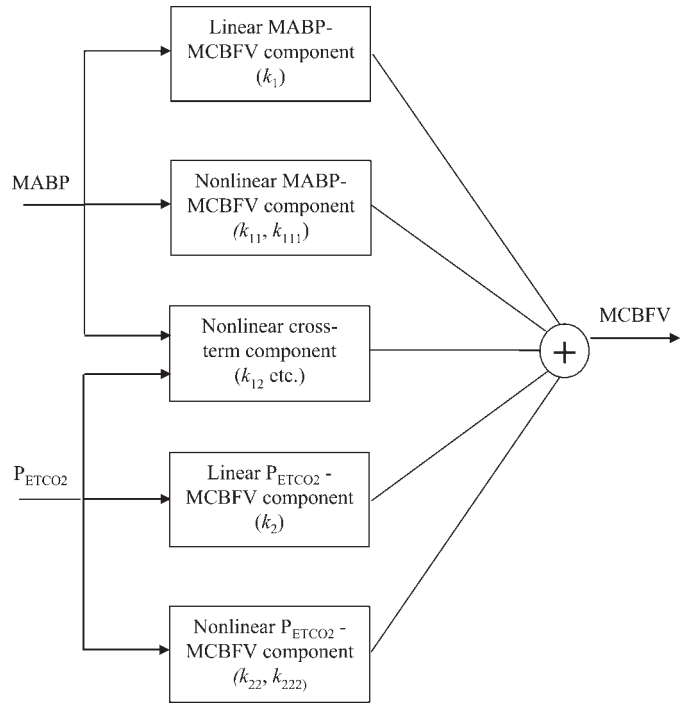
Fig. 1. Nonlinear model of the dynamic effects of mean arterial blood pressure (MABP) and end-tidal CO_2 ($P_{ET_{CO_2}}$) on mean cerebral blood flow velocity (MCBFV). The linear components correspond to the first-order terms in *Eq. 1* (i.e., k_1 and k_2 for MABP and $P_{ET_{CO_2}}$, respectively). The nonlinear components correspond to the second- and third-order terms in *Eq. 1* with $i_1 = i_2$ (i.e., k_{11}, k_{111}, k_{22}, and k_{222}) and the nonlinear cross-term components correspond to the second- and third-order terms with $i_1 \neq i_2$ (i.e., k_{12}, etc.).

The MI-LVN is equivalent to the general Volterra model of a nonlinear multiple-input system, given below for a two-input, Qth-order system:

$$y(n) = k_0 + \sum_{i=1}^{2} \sum_{m_1} k_i(m_1)x_i(n - m_1) +$$
$$+ \sum_{i_1=1}^{2} \sum_{i_2=1}^{2} \left\{ \sum_{m_1} \sum_{m_2} k_{i_1 i_2}(m_1, m_2)x_{i_1}(n - m_1)x_{i_2}(n - m_2) \right\} + \ldots \quad (1)$$
$$+ \sum_{i_1=1}^{2} \ldots \sum_{i_Q=1}^{2} \left\{ \sum_{m_1} \ldots \sum_{m_Q} k_{i_1 \ldots i_Q}(m_1, m_Q)x_{i_1}(n - m_1) \ldots x_{i_Q}(n - m_Q) \right\}$$

where $x_1(n)$ and $x_2(n)$ are the two inputs of the system (i.e., MABP and $P_{ET_{CO_2}}$, respectively), $y(n)$ is the system output (i.e., MCBFV), and $k_{i_1 \ldots i_Q}$ denote the Qth-order Volterra kernels of the system corresponding to inputs $i_1 \ldots i_Q$. If $i_1 = \ldots = i_Q = i$, $k_{i \ldots i}$ denote the Qth-order, ith input self-kernels and describe the linear ($Q = 1$) and nonlinear ($Q > 1$) effects of the Q past values of the ith input at time lags ($m_1, m_2, \ldots, m_Q$) before the time lag n at which the output is computed. If some of $i_1 \ldots i_Q$ are different, $k_{i_1 \ldots i_Q}$ denote the Qth-order cross-kernels, which describe the nonlinear interactions between past values of the two inputs at the corresponding time lags. The Volterra kernels in *Eq. 1* can be expressed in terms of the LVN parameters, which are in turn estimated via an iterative gradient descent scheme from the input-output data (32). In our case, the dynamic effects of MABP on MCBFV (dynamic cerebral autoregulation) are described by $k_{i \ldots i}$ for $i = 1$ in *Eq. 1* and correspond to the upper two blocks of Fig. 1, whereas the effects of $P_{ET_{CO_2}}$ (cerebral vasomotor reactivity) are described by $k_{i \ldots i}$ for $i = 2$ in *Eq. 1* and correspond to the lower two blocks of Fig. 1. The nonlinear interaction terms between MABP and $P_{ET_{CO_2}}$ (cross-kernels) constitute the middle block in Fig. 1. Further details on the methodology are provided in Refs. 31 and 32.

The structural parameters of the MI-LVN were selected on the basis of the normalized mean-square error (NMSE) of the output prediction achieved by the model for a validation data set (i.e., data not used for training). The output prediction NMSE is defined as the sum of squares of the model residuals (defined as the difference between the model prediction and the true MCBFV output) divided by the corresponding mean-squared true MCBFV output. The statistical significance of the validation NMSE for various model structures was assessed by comparing the NMSE reduction achieved by more complex models (i.e., NMSE$_{complex}$ − NMSE$_{simple}$, where NMSE$_{complex}$ and NMSE$_{simple}$ are the NMSEs corresponding to the complex and simple model structures, respectively) to the a-percentile value of a χ^2 distribution with Δp degrees of freedom, where Δp is the difference in the number of free parameters between different models. Specifically, the quantity $N \cdot (\text{NMSE}_{complex} - \text{NMSE}_{simple})/\text{NMSE}_{complex}$, where N denotes the number of validation data points, was compared with $\chi^2_a(\Delta p)$, with the significance level set at 0.05 (50). Of the 6-min data segments (360 points) that were available for each LBNP level, 320

points were used to train the network, and the rest were used for validation purposes.

The first-order MABP and $P_{ET_{CO_2}}$ kernels (k_1 and k_2, respectively) were computed in the time and frequency domains and subsequently group averaged. The second-order MABP and $P_{ET_{CO_2}}$ self-kernels were obtained in the frequency domain after applying the two-dimensional fast Fourier transform to k_{11} and k_{22}, respectively. To assess the effects of orthostatic stress on the second-order dynamics, we calculated the corresponding SSP at each LBNP level by integrating the second-order frequency responses in the two-dimensional frequency domain, with the ranges defined as above (i.e., VLF: [0.005, 0.005] to [0.04, 0.04] Hz, LF: [0.04, 0.04] to [0.15, 0.15] Hz and HF: [0.15, 0.15] to [0.3, 0.3] Hz), and group-averaged the results. The SSP of the model prediction and its MABP and $P_{ET_{CO_2}}$ components (*top* two and *bottom* two blocks in Fig. 1, respectively) was also calculated by integrating the corresponding PSD functions for all subjects. This yielded an indirect measure of the third-order dynamics included in the model.

Finally, to illustrate the effects of orthostatic stress on the MCBFV response to a controlled pressure stimulus over the entire frequency range of interest, we calculated the amplitude of the MI-LVN model responses to simulated sinusoidal MABP stimuli at baseline and during LBNP, and the results were averaged for all subjects. The amplitude of the simulated MABP signal was 2 mmHg peak to peak, and its frequency was varied from 0.01 to 0.3 Hz in steps of 0.01 Hz.

RESULTS

All ten subjects withstood the LBNP up to −40 mmHg. Seven of the ten withstood the LBNP test up to −50 mmHg, five up to −60 mmHg, and three up to −70 mmHg. Hence, group-averaged results are given up to −50 mmHg LBNP. Changes in steady-state cerebral and systemic hemodynamics and their overall variabilities during LBNP are given in Table 1. Steady-state MABP remained relatively constant during LBNP, whereas steady-state MCBFV and $P_{ET_{CO_2}}$ decreased and HR increased at high levels of LBNP (Table 1). MABP and MCBFV variabilities remained unchanged, whereas $P_{ET_{CO_2}}$ and HR variabilities increased considerably during LBNP ($P < 0.05$ at −40 and −50 mmHg, Table 1).

Typical time series of MABP, $P_{ET_{CO_2}}$, and MCBFV at baseline and during LBNP employed for model estimation are shown in Fig. 2. Note the large and simultaneous slow drops with a period of ∼100 s in $P_{ET_{CO_2}}$ and MCBFV at −40 and −50 mmHg LBNP, which are absent in the MABP time series. These slow, concurrent $P_{ET_{CO_2}}$ and MCBFV variations were observed for several subjects.

Table 1. *Changes in systemic and cerebral hemodynamics during lower body negative pressure*

LBNP, mmHg	Mean Value				Variability			
	MABP, mmHg	MCBFV, cm/s	$P_{ET_{CO_2}}$, Torr	HR, beats/min	MABP, mmHg	MCBFV, cm/s	$P_{ET_{CO_2}}$, Torr	HR, beats/min
0	88.4±5.3	70.5±6.1	30.5±0.9	62.1±3.8	4.6±0.4	5.4±0.5	1.6±0.4	3.7±0.4
−15	88.6±5.2	68.7±6.3	29.5±1.5	62.8±3.1	4.4±0.5	5.1±0.8	2.4±0.8	4.1±0.5
−30	88.4±4.3	66.5±6.0*	27.1±2.7	68.5±3.9	4.3±0.5	5.0±0.4	2.2±0.3	4.1±0.5
−40	88.3±4.6	60.7±6.1*	25.2±2.4*	76.1±4.5*	4.7±0.5	5.2±0.5	2.6±0.3*	5.0±0.5*
−50	86.5±4.4	56.1±7.2*	23.4±3.2*	81.3±4.4*	4.9±0.6	5.7±0.6	2.8±0.4*	5.7±0.9*

Values are means ± SE. LBNP, lower-body negative pressure; MABP, mean arterial blood pressure; MCBFV, mean cerebral blood flow velocity; $P_{ET_{CO_2}}$, end-tidal CO_2; HR, heart rate. Variability was computed as standard deviation around the mean value of the 6-min data segments. *$P < 0.05$ compared with baseline.
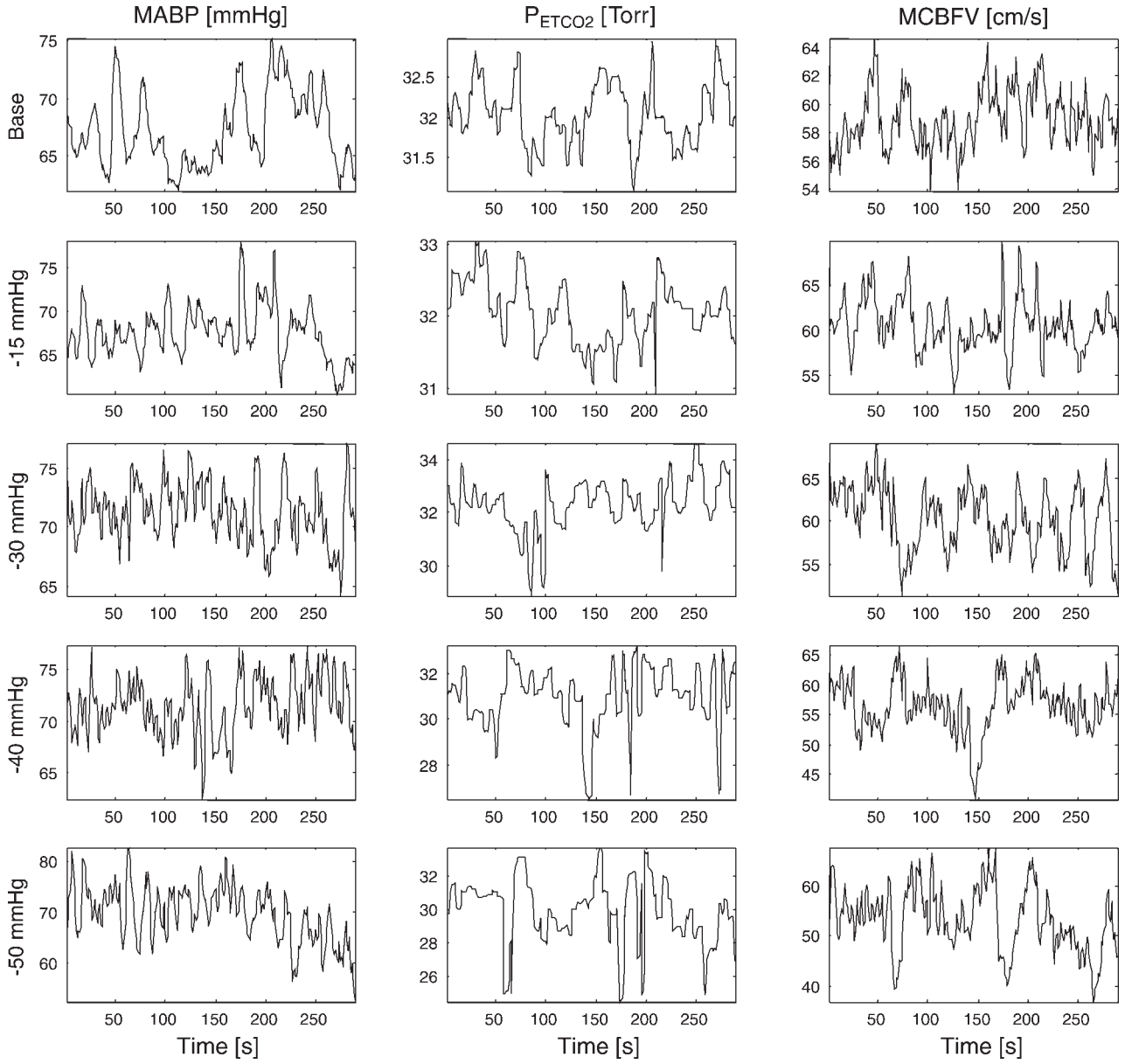
Fig. 2. Typical segments of MABP (mmHg), P_{ETCO_2} (Torr), and MCBFV (cm/s) time series employed to assess dynamic cerebral autoregulation and cerebral vasomotor reactivity, at baseline and during lower body negative pressure (LBNP).

The estimated output prediction NMSEs for the validation data sets are given in Table 2 for one- and two-input (whereby MABP or MABP and P_{ETCO_2} were the model inputs, respectively), as well as for linear and nonlinear (whereby only linear kernels or nonlinear kernels up to third order were used to fit the input-output data, i.e., $Q = 1$ and $Q = 3$ in *Eq. 1*, respectively) MI-LVN models. The improvement achieved by using nonlinear models in terms of model performance was assessed by the resulting NMSE reduction, which was significant at all levels of LBNP, ranging from around 12% to above 25% for two-input models. The incorporation of P_{ETCO_2} improved the performance of the MI-LVN model further, as indicated by the corresponding NMSE reduction, which ranged from 12% to almost 30% for nonlinear models.

The relative contributions of the linear and nonlinear model terms as well as that of the MABP and P_{ETCO_2} terms are illustrated in Fig. 3 at -50 mmHg in the time and frequency domains. In the *bottom left*, the cross-term component (*bottom* trace) corresponds to the nonlinear interactions between the two inputs (*middle* block in Fig. 1). In the *top right*, the first-order residuals are defined as the difference between the actual MCBFV output $y(n)$ and the linear prediction component $\tilde{y}_1(n)$:

$$e_1(n) = y(n) - \tilde{y}_1(n) = y(n) - \left[k_0 + \sum_{i=1}^{2} \sum_{m_1} k_i(m_1) x_i(n - m_1) \right] \quad (2)$$

whereas the total residuals are defined as the difference between the actual output and the total model prediction $\tilde{y}(n)$,

Table 2. *Normalized mean square prediction error for the validation data for 1-input (MABP)
and 2-input (MABP and $P_{ET_{CO_2}}$) LVN models*

	MABP		MABP and $P_{ET_{CO_2}}$	
	Linear ($Q = 1$) NMSE	Nonlinear ($Q = 3$) NMSE	Linear ($Q = 1$) NMSE	Nonlinear ($Q = 3$) NMSE
Baseline	53.5 ± 9.4	46.5 ± 7.9	40.5 ± 9.5	17.3 ± 4.2*†
-15 mmHg	61.2 ± 8.4	54.6 ± 6.0	49.4 ± 7.7	32.6 ± 4.0*†
-30 mmHg	56.5 ± 8.5	43.3 ± 5.4*	47.9 ± 7.2†	21.1 ± 3.4*†
-40 mmHg	48.0 ± 9.2	36.0 ± 5.8*	34.6 ± 5.7	23.2 ± 5.1*†
-50 mmHg	45.8 ± 9.0	35.7 ± 6.8*	36.5 ± 5.3	23.7 ± 6.2*†

Values are means $\pm$ SE. NMSE, normalized mean-square error. *$P < 0.05$, nonlinear vs. linear models. †$P < 0.05$, 2-input vs. 1-input models.

whereby all model terms up to third order are taken into account:

$$e_{tot}(n) = y(n) - \tilde{y}(n) = y(n) - \left(k_0 + \sum_{q=1}^{3} \left\{ \sum_{i_1=1}^{2} \ldots \right. \right.$$

$$\sum_{i_q=1}^{2} \left[\sum_{m_1} \ldots \sum_{m_q} k_{i_1 \ldots i_q}(m_1, \ldots, m_q) x_{i_1}(n - m_1) \ldots x_{i_q}(n - m_q) \right] \left. \left. \right\} \right) \quad (3)$$

The shaded area denotes the improvement achieved by the nonlinear terms in the frequency domain. The MABP residuals (*bottom right*) are defined as the difference between actual MCBFV output and MABP output component (given by *Eq. 3*, but for $i_1 = i_2 = i_q = 1$); hence the shaded area denotes the improvement achieved by the $P_{ET_{CO_2}}$ terms. From the time-domain plots, it is evident that the model prediction was very close to the true output, as indicated also by the achieved NMSE for this data segment (14%). The nonlinear terms, the $P_{ET_{CO_2}}$ terms, as well as the cross-terms account for a considerable fraction of the slow MCBFV variations. This is further illustrated by the form of the shaded areas in the frequency domain plots, the power of which lies mainly in the VLF range. Note the pronounced slow MCBFV fluctuations at -50 mmHg LBNP (peaking at 0.01 Hz), which are accounted for by the $P_{ET_{CO_2}}$ terms. The VLF and LF effects of the nonlinear and $P_{ET_{CO_2}}$ model terms were found to be consistent among all subjects and levels of LBNP (for further comparisons to baseline conditions, the reader is referred to Ref. 34).
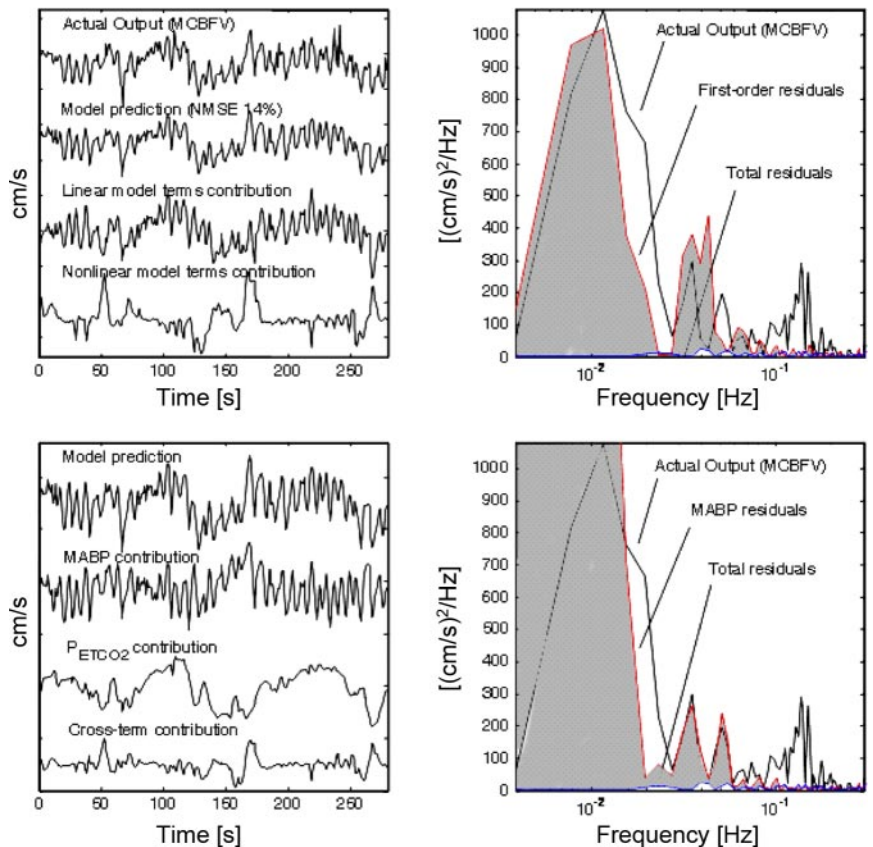

Fig. 3. *Left*: actual MCBFV output and Laguerre-Volterra network (LVN) model prediction (*top*: total, linear and nonlinear terms; *bottom*: total, MABP, $P_{ET_{CO_2}}$, and cross-terms) for a typical data segment at -50 mmHg. *Right*: spectra of actual output and model residuals (*top*: linear and total; *bottom*: MABP and total). Shaded areas denote the effect of the nonlinear and $P_{ET_{CO_2}}$ terms in the frequency domain, respectively.

The group-averaged first-order MABP and $P_{ET_{CO_2}}$ kernels (k_1 and k_2 in *Eq. 1*), which describe the linear component of the dynamic effects of MABP and $P_{ET_{CO_2}}$ on MCBFV, are shown in Figs. 4 and 5, respectively, in the frequency domain. The linear kernels operate on the system input in the same manner to the impulse response function for linear systems (30). However, it should be noted that, in the case of nonlinear systems, the linear kernels are not equivalent to the system impulse response, because the latter depends on the diagonal points of the higher-order kernels as well. The VLF magnitude of the MABP kernel increased gradually during LBNP, whereas the LF and HF magnitudes remained relatively unchanged. Consequently, the high-pass characteristic of the MABP linear frequency response at baseline was gradually altered to a band-stop characteristic at high levels of LBNP (i.e., high VLF, HF magnitude values, low LF magnitude values; Fig. 4). The $P_{ET_{CO_2}}$ kernel exhibited a low-pass characteristic at baseline and during LBNP, implying that slow variations of $P_{ET_{CO_2}}$ had a larger impact on MCBFV than fast variations. However, the magnitude of the $P_{ET_{CO_2}}$ linear frequency response decreased with increasing LBNP (Fig. 5).

Representative second-order self-kernels (k_{11} and k_{22} in *Eq. 1*) at baseline and -50 mmHg LBNP are shown in Fig. 6. Note that the second-order self-kernels are symmetric with respect to their arguments in both the time and frequency domains. Their diagonal values describe the quadratic effects, i.e., squared

values, of past input (MABP or $P_{ET_{CO_2}}$) values on MCBFV, whereas the off-diagonal values describe the effects of interactions (i.e., pair products) between past input values at different times on MCBFV. In an analogous manner, the diagonal elements of the second-order frequency responses describe the quadratic effects of specific input spectral components and the off-diagonal elements describe the effects of nonlinear interactions between different input spectral components on MCBFV. Most of the second-order kernel power resides in the VLF range in the two-dimensional frequency domain, in agreement with Fig. 3. At baseline, the MABP response exhibited a main diagonal spectral peak at [0.02, 0.02] Hz and a secondary off-diagonal peak at [0.008, 0.1] Hz, whereas the $P_{ET_{CO_2}}$ response exhibited a main diagonal peak at [0.025, 0.025] Hz and an off-diagonal peak at [0, 0.025] Hz. At -50 mmHg, the main diagonal peaks were shifted to lower frequencies and the off-diagonal peaks were not as discernible, especially for $P_{ET_{CO_2}}$. The VLF magnitude of the second-order MABP frequency response increased with LBNP, in contrast to its $P_{ET_{CO_2}}$ counterpart, which decreased markedly (Fig. 6). These observations were consistent among different subjects, as shown in Fig. 7, where the group-averaged SSP of the second-order frequency responses is plotted as a function of LBNP level. The second-order dynamics were affected similarly to the first-order dynamics (Figs. 4–5); an increasing trend was observed for the k_{11} VLF SSP ($P < 0.05$ at -40 mmHg),
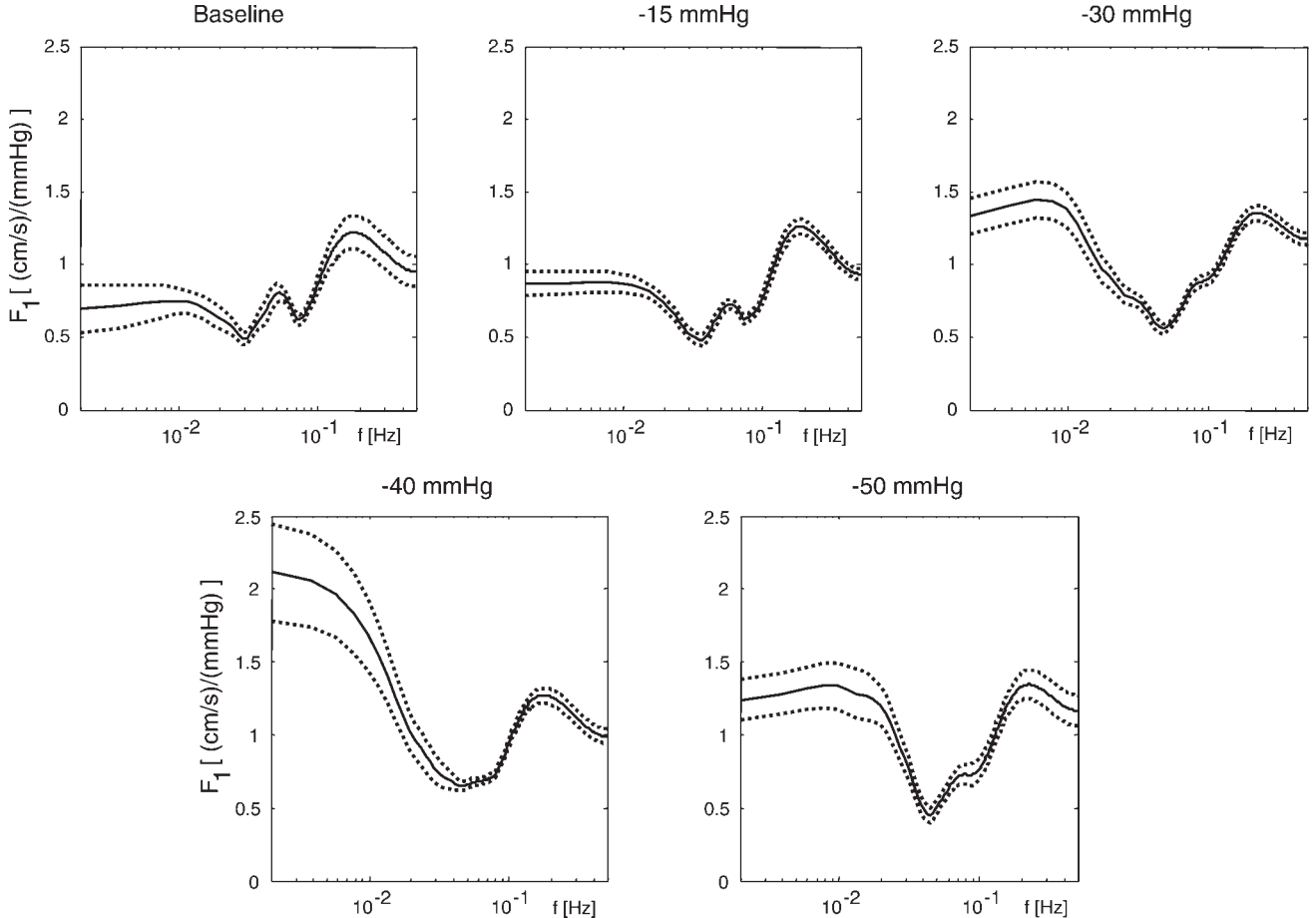

Fig. 4. Group-averaged first-order MABP kernels in the frequency domain (F_1) at baseline and during LBNP (solid line: mean value, dotted line: SE). Note the increase in very-low-frequency (VLF) magnitude during LBNP.
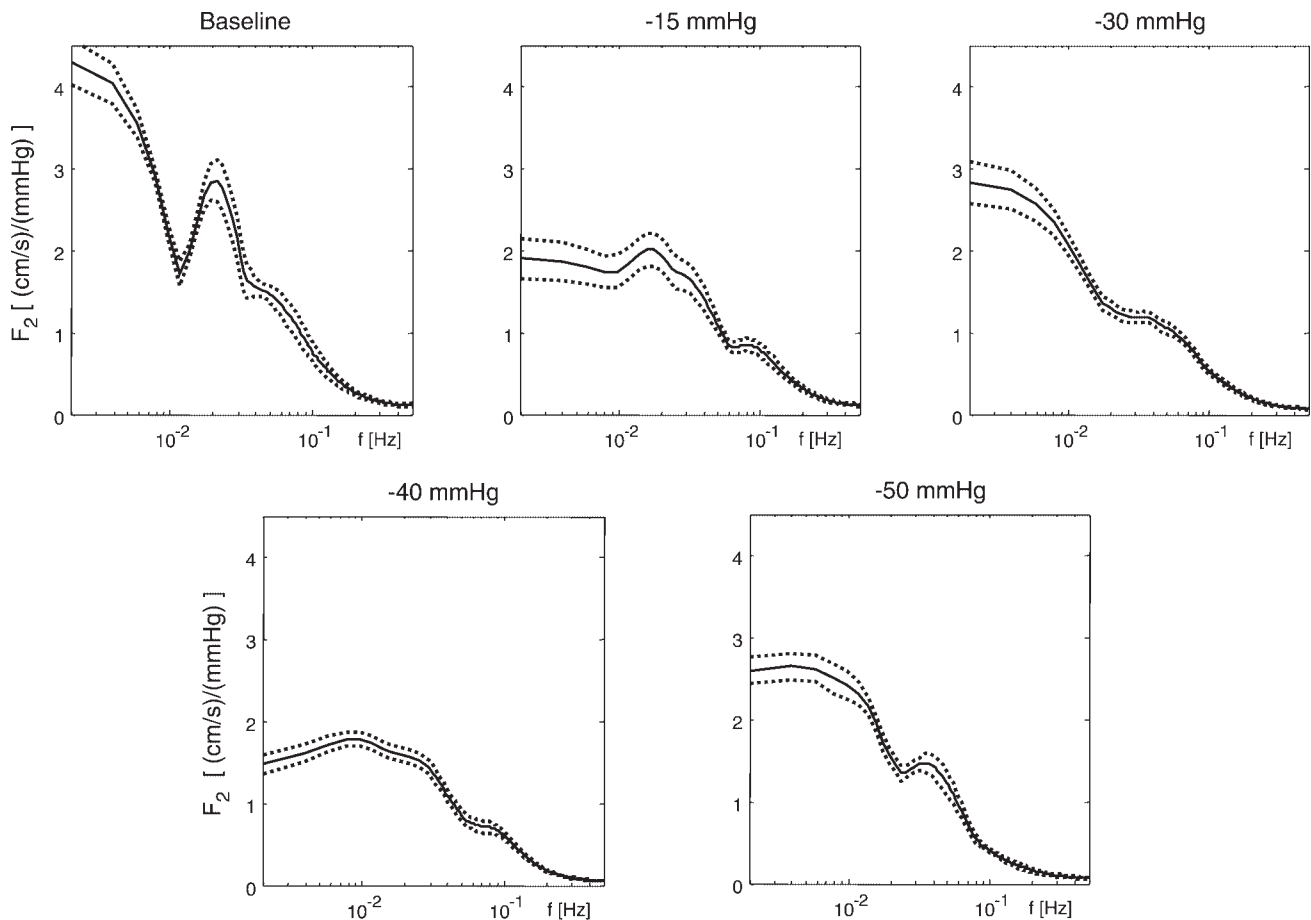
Fig. 5. Group-averaged first-order $P_{ET_{CO_2}}$ kernels in the frequency domain (F_2) at baseline and during LBNP (solid line, mean value; dotted lines, SE). Note the decrease in the kernel magnitude during LBNP.

whereas the LF and HF power remained unchanged. On the other hand, the $P_{ET_{CO_2}}$ second-order kernel SSP decreased during LBNP ($P < 0.05$ at -50 mmHg in the VLF and LF ranges and also at -40 mmHg in the VLF range).

The group-averaged SSP of the model prediction and its MABP and $P_{ET_{CO_2}}$ components (*top* two and *bottom* two blocks in Fig. 1) at baseline and during LBNP are shown in Fig. 8, along with the SSP of the MABP and $P_{ET_{CO_2}}$ inputs. The model prediction power depends on all model terms (zeroth to third order) and on the power of the two inputs, as shown by *Eq. 1*. Therefore, it yields an indirect way to examine the effects of LBNP on the third-order model dynamics, because the latter would have to be plotted as a series of two-dimensional "slices" otherwise. Despite an initial decrease up to -30 mmHg LBNP, which concurred with a decrease in the VLF MABP input power, the VLF SSP of the MABP model prediction component returned to its baseline levels at -40 and -50 mmHg LBNP, even though the MABP SSP decreased further (Fig. 8; *top left*). The power ratio (PR) of the VLF MABP model prediction component SSP to the corresponding MABP input SSP increased from 0.6 at baseline to 1.7 at -50 mmHg LBNP. On the other hand, the PR remained relatively constant in the LF and HF ranges. The high PR values in the HF range (between 1 and 1.2) indicate that HF MABP variations are attenuated less effectively both at baseline and during LBNP.

MABP variations accounted for almost all the MCBFV changes in the HF range, as shown in the *right* panels of Fig. 8. On the other hand, $P_{ET_{CO_2}}$ had a considerable effect in the VLF and LF ranges. The VLF SSP of both $P_{ET_{CO_2}}$ input and its corresponding model prediction component increased gradually during LBNP (Fig. 8). However, the VLF $P_{ET_{CO_2}}$ PR is highest at baseline and was reduced during LBNP, in agreement with the magnitude reduction observed for the first- and second-order $P_{ET_{CO_2}}$ frequency responses. Despite this reduction, a gradually increasing fraction of the VLF MCBFV variations was explained by $P_{ET_{CO_2}}$ changes during LBNP, owing to the significantly increased $P_{ET_{CO_2}}$ variability under these conditions. Note that, whereas the VLF $P_{ET_{CO_2}}$ and MABP contributions to the model prediction were approximately equal at baseline, the $P_{ET_{CO_2}}$ contribution was almost three times that of MABP at -50 mmHg LBNP. In the LF range, the $P_{ET_{CO_2}}$ contribution SSP remained approximately constant and equal to its MABP counterpart during LBNP (Fig. 8).

The above results suggest that VLF MABP variations were attenuated less effectively during LBNP compared with baseline, because both the linear (assessed by the first-order kernels) and nonlinear (assessed by the second-order kernels and PR) components of the MABP-MCBFV relationship increased at high LBNP levels. On the other hand, effective regulation of LF MABP variations was maintained during LBNP. Cerebral
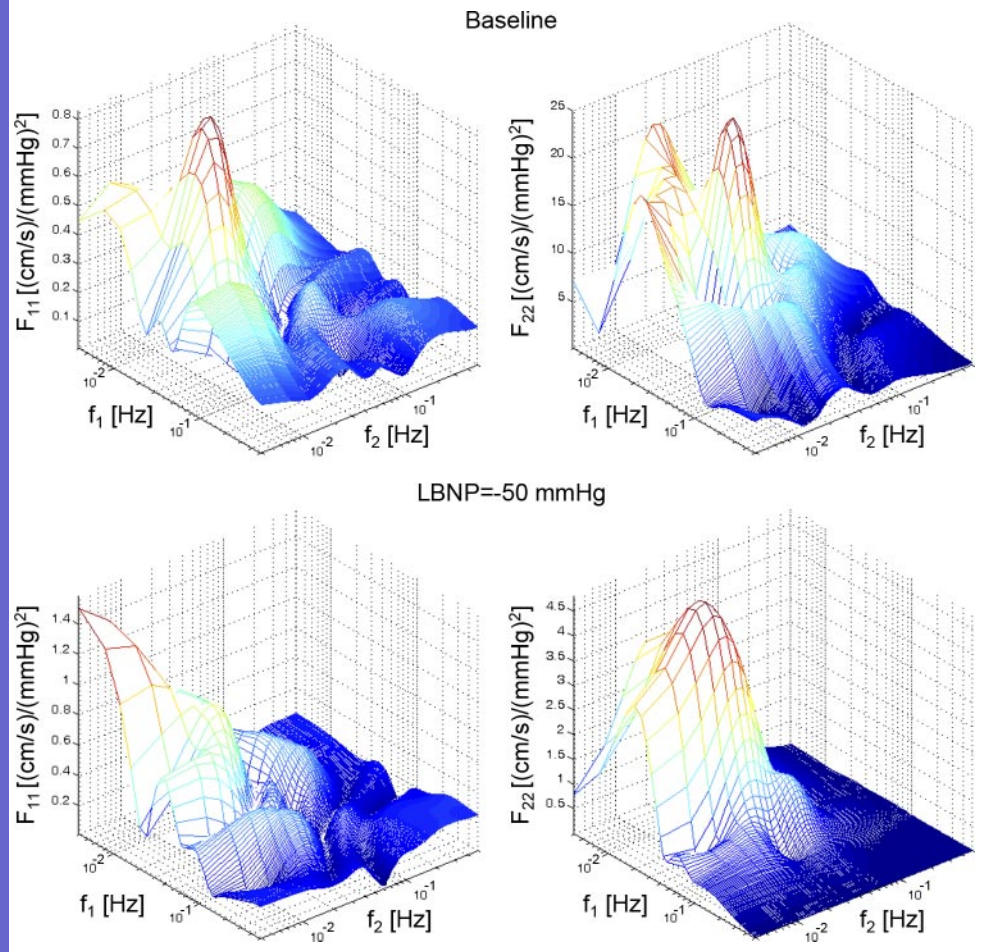
Fig. 6. Typical second-order MABP (*left*) and $P_{ET_{CO_2}}$ (*right*) kernels in the frequency domain at baseline and -50 mmHg LBNP. Note the increase in the magnitude of the second-order MABP frequency response and the decrease in the magnitude of the second-order $P_{ET_{CO_2}}$ frequency response during LBNP.

vasomotor reactivity to VLF and LF $P_{ET_{CO_2}}$ changes was found to be decreased during LBNP, although the increase in VLF $P_{ET_{CO_2}}$ variability resulted in more pronounced CO_2 effects on MCBFV variations.

Finally, the averaged amplitudes of the MI-LVN model response to the unit-amplitude simulated sinusoidal MABP

stimuli for frequencies between 0.01 and 0.3 Hz are shown in Fig. 9. The low amplitude values in the VLF and LF ranges at baseline demonstrate the high-pass characteristics of dynamic autoregulation under these conditions. During LBNP, the VLF output amplitudes increased markedly, suggesting less effective attenuation of VLF MABP variations. The most effective
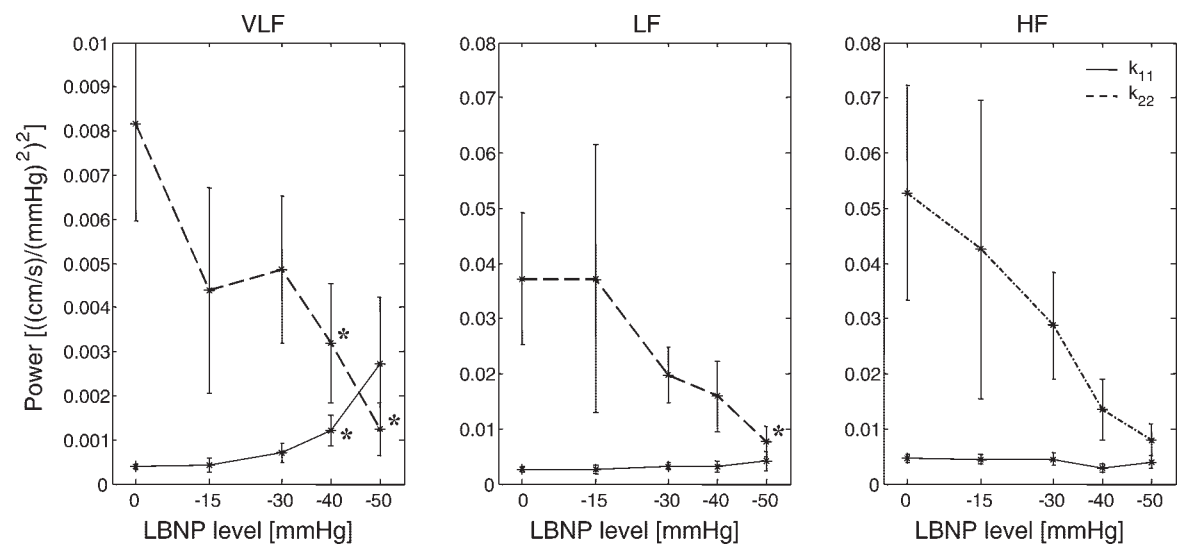

Fig. 7. Group-averaged segmental spectral power (SSP; mean $\pm$ SE) of the second-order MABP (k_{11}, solid line) and $P_{ET_{CO_2}}$ kernels (k_{22}, dashed line) at baseline and during LBNP. *$P < 0.05$ compared with baseline.
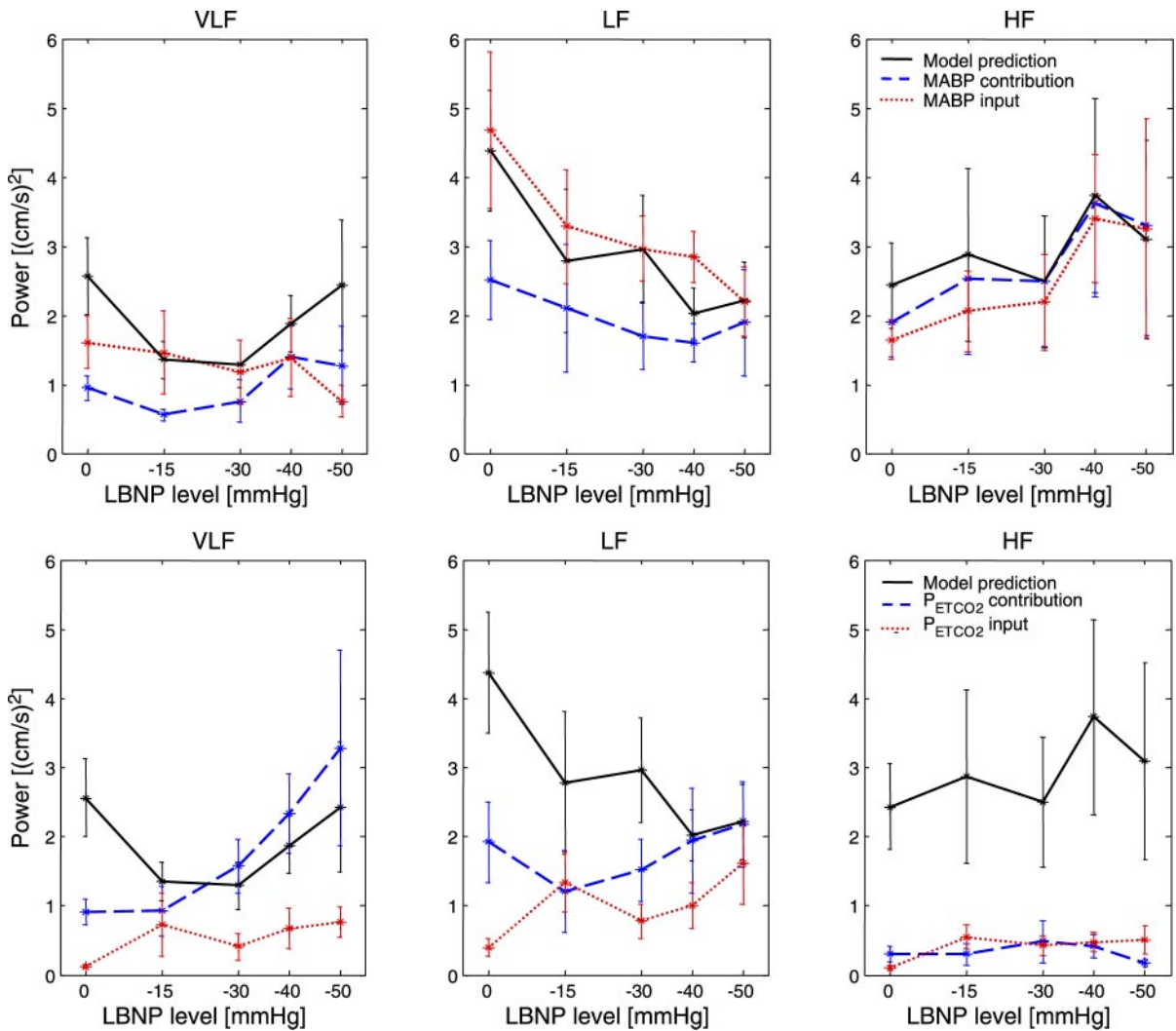
Fig. 8. Group-averaged SSP of total model prediction (black solid line) along with MABP input (red dotted line; *top*) and MABP output component (blue dashed line) SSP and P_{ETCO_2} input (red dotted line) and P_{ETCO_2} output component (blue dashed line) SSP (*bottom*). Values are means $\pm$ SE. Note the increase in the VLF power of MABP contribution for high levels of LBNP and the increase in the VLF power of both P_{ETCO_2} input and P_{ETCO_2} output component.

attenuation was observed between 0.04 and 0.07 Hz in the LF range. Overall, the simulation results are consistent with the experimental findings of this study.

DISCUSSION

The major findings of the present study are threefold: *1*) By employing a multiple-input and nonlinear methodology we were able to quantify cerebral hemodynamics at baseline and during LBNP over the entire frequency range of the naturally occurring hemodynamic signal variabilities (0.005–0.3 Hz). Subsequently, we were able to simultaneously identify changes in cerebral dynamic autoregulation and cerebral vasomotor reactivity during LBNP in the VLF range for the first time. Nonlinearities were found to be significant and mainly active in the VLF range at all levels of LBNP. *2*) Dynamic cerebral autoregulation, which was assessed by the first- and second-order MABP Volterra kernels of the model as well as by the MABP model prediction component, was found to be impaired in the VLF range during LBNP. *3*) Cerebral vasomotor reactivity in response to spontaneous variations of P_{ETCO_2}, which

was assessed by the P_{ETCO_2} Volterra kernels and the corresponding model prediction component, was attenuated during LBNP. However, P_{ETCO_2} variability in the VLF range increased considerably during LBNP and accounted for a larger fraction of VLF MCBFV changes compared with the baseline.

Collectively, these findings document the presence of altered cerebral hemodynamics in humans during LBNP. We speculate that these changes reflect a progressively reduced cerebrovascular reserve to compensate for the instability of the systemic circulation during orthostatic stress, which, combined with the decrease observed in the MCBFV steady-state value, may ultimately lead to cerebral hypoperfusion and syncope.

The Volterra-Wiener approach has been employed extensively for modeling physiological systems (30). It is well suited to the complexity of such systems because it yields rigorous mathematical descriptions of their dynamic behavior by utilizing input-output data, without requiring any a priori assumptions about system structure. Specifically, nonlinear techniques have been employed successfully for modeling renal (8, 9) and cerebral (33, 34, 38) autoregulation, as well as the nonlinear
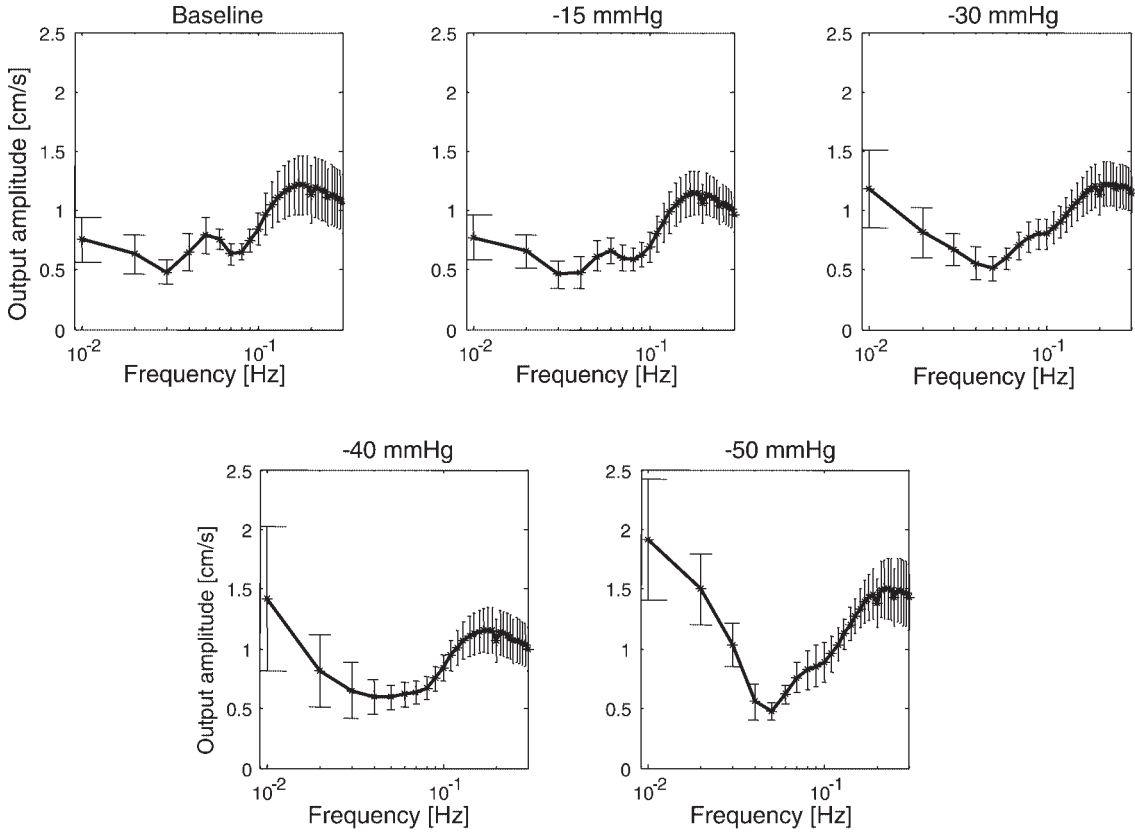
Fig. 9. Group-averaged multiple-input LVN output amplitudes in response to sinusoidal MABP stimuli with unit amplitude and varying frequencies. Note the increase in the model output amplitude in the VLF range. Error bars denote SE of group-averaged data.

properties of cardiovascular variability (7, 55). The advantage of the LVN methodology is that it achieves accurate modeling of nonlinear systems by utilizing short-input data records and a substantially smaller number of free parameters compared with other techniques, such as cross-correlation, orthogonal approaches, or standard functional expansions. Whereas this number depends exponentially on the system order for these approaches, the same dependence is linear for the LVN approach, constituting it an ideal choice for high-order and multiple-input systems (31, 32), such as in the present study.

The general Volterra model of *Eq. 1* can be viewed as a generalization of the convolution sum, which describes the dynamic input-output relationship for linear systems (30), to nonlinear systems. The first-order (linear) Volterra kernels describe the linear effects of system inputs on the output, and the nonlinear (Qth order, where $Q > 1$) kernels describe the effect of the interaction of the Q past values of an input (or the interactions between different inputs in the case of cross-kernels) on the system output. As mentioned before, however, the first-order Volterra kernel is not equivalent to the system impulse response. Also, whereas the response of a linear system to a sinusoidal stimulus is a (scaled) sinusoid of the same frequency, the response of a nonlinear system exhibits the input (fundamental) frequency as well as harmonics due to the higher-order kernels, scaled by the magnitude of the diagonal elements of the corresponding frequency responses (30).

The changes in cerebral hemodynamics during LBNP were assessed quantitatively over the three frequency ranges of interest by integrating the spectral power of the input, output,

and model-prediction signals. The limits of the three frequency ranges were selected on the basis of the frequency-domain characteristics of cerebral hemodynamics observed in the present and previous studies (33, 34, 53), which demonstrated the significant effects of nonlinearities and CO_2 below 0.04 Hz. The use of three distinct frequency regions, albeit with different limits, has been also adopted in other studies (12, 53).

The model nonlinearities were found to be prominent in the VLF range (below 0.04 Hz), both under resting conditions and during LBNP. By incorporating spontaneous variations of $P_{ET_{CO_2}}$ in a two-input LVN model, we were able to quantify the dynamic effects of MABP and end-tidal CO_2 on MCBFV variations simultaneously. The performance of the model was improved significantly in terms of achieved prediction NMSE when two inputs were employed, compared with one-input models (Table 2). The dynamics between $P_{ET_{CO_2}}$ and MCFBV were characterized by strong nonlinearities, as reported previously as well (34). The effects of $P_{ET_{CO_2}}$ variations were observed mainly in the VLF and LF ranges, and their relative contributions increased considerably during LBNP, as shown by the spectral power of the MABP and $P_{ET_{CO_2}}$ model prediction components (Fig. 8). At high levels of LBNP, the $P_{ET_{CO_2}}$ contribution in the VLF range (assessed by the corresponding SSP) exceeded that of MABP, accounting for most of the VLF MCFBV variability.

The above observations are consistent with previous results obtained under resting conditions (33, 34) and demonstrate that the low coherence values between MABP and MCBFV (below 0.5) in the VLF range (52, 53) are due to the presence of strong

dynamic nonlinearities between MABP and MCBFV as well as to the effects of CO_2. Therefore, modeling cerebral hemodynamics in this frequency range by linear techniques alone and/or without taking into account the CO_2 effects is not sufficient (28). As a result, in previous studies of dynamic cerebral autoregulation under orthostatic stress based on transfer function analysis between MABP and MCBFV variations (47, 53), its characteristics were not examined in the VLF range.

The VLF magnitude of the first-order MABP kernels and the SSP of the second-order MABP kernels and model prediction components increased substantially at high levels of LBNP, suggesting that both the linear and nonlinear effects of slow MABP variations on MCBFV changes were more pronounced. This suggests that the effects of VLF MABP variations on MCBFV were not regulated effectively and that dynamic cerebral autoregulation was impaired in the VLF range. These observations extend our previous studies of dynamic cerebral autoregulation using linear transfer function analysis (53), whereby a significant increase in the LF transfer function gain (~25%) was reported at high levels of LBNP. A direct comparison, however, should be made with caution, because the limits of the frequency ranges are different and autoregulation dynamics were not obtained below 0.07 Hz in Ref. 53.

It remains controversial whether dynamic cerebral autoregulation is altered under orthostatic stress (6, 10, 12, 46, 47, 53). In the present study as well as in Ref. 53, autoregulatory function was found to be impaired at high levels of LBNP, and similar findings were reported during HUT (12). Moreover, autoregulation, quantified by using a "dynamic autoregulatory index," although initially preserved during HUT, was found to become dramatically impaired immediately before tilt-induced syncope in volunteers with or without a history of recurrent vasovagal syncope (6). On the other hand, dynamic autoregulation was found to remain unchanged in normal and neurally mediated syncope patients during HUT (46, 47). One reason for these discrepancies is likely to be the different experimental methods used (LBNP vs. HUT), as well as the timing of assessment (before or during the throes of syncope induced by orthostatic stress). The amount of orthostatic stress during HUT may not be equivalent to high levels of LBNP. Moreover, HUT stimulates the vestibulosympathetic reflex, which may elicit cerebral hemodynamic responses different from those during LBNP (22, 44). Another reason may be the use of different modeling approaches. For example, in a recent study, dynamic cerebral autoregulation was assessed by the relationship between beat-to-beat values of MABP and cerebrovascular resistance, which was defined as the ratio of MABP over MCBFV, to alleviate the limited reliability of transfer function estimates between MABP and MCBFV in the VLF range (12). This relationship exhibited sufficiently high coherence values in the VLF range; however, this is to be expected because the derived cerebrovascular resistance index is directly proportional to the changes in MABP. A significantly reduced transfer function gain between MABP and cerebrovascular resistance index in the frequency range between 0.03 and 0.2 Hz was observed during HUT, which has been interpreted to indicate impaired dynamic cerebral autoregulation during HUT (12). In another study, the MABP and MCBFV signals were high-passed at 0.02 Hz before transfer function estimation (47).

Finally, transfer function estimates between MABP and MCBFV were only considered above 0.07 Hz in Ref. 53. Therefore, dynamic autoregulation was not assessed in the VLF range, where most of the changes during LBNP were observed in the present study. The latter was made possible by the proposed multiple-input and nonlinear methodology, which allowed us to quantify cerebral hemodynamics in the VLF range and to identify changes in dynamic cerebral autoregulation and cerebral vasomotor reactivity simultaneously during LBNP.

The effect of orthostatic stress on cerebral vasomotor reactivity has been studied previously under steady-state conditions (21, 25). Cerebral vasomotor reactivity was found to be reduced during HUT and enhanced during autonomic ganglionic blockade (21). Specifically, it was found that the linear regression slope of the steady-state changes in MCBFV vs. changes in $P_{ET_{CO_2}}$ elicited by hyperventilation and CO_2 breathing (5%) was increased after ganglionic blockade, suggesting that sympathetic neural activity has a constraining effect on the CBF responses to CO_2 stimuli during HUT (21). However, under similar experimental conditions of changes in breathing CO_2, cerebral vasomotor reactivity remained unaffected during LBNP (25). These differences reflect the long-standing controversy about the role of autonomic neural activity in the control of CBF in humans (17, 43, 54).

In the present study, we examined the effects of orthostatic stress on dynamic cerebral vasomotor reactivity in response to spontaneous changes in $P_{ET_{CO_2}}$. CO_2 reactivity was assessed by the first- and second-order $P_{ET_{CO_2}}$ kernels, as well as by the $P_{ET_{CO_2}}$ model prediction components, and was found to be reduced during LBNP. We speculate that augmented sympathetic neural activity during LBNP attenuates dynamic MCBFV responses to breath-by-breath oscillations in $P_{ET_{CO_2}}$ (21, 54). Despite these changes, the overall effects of $P_{ET_{CO_2}}$ on changes in MCBFV were more pronounced because of the marked increase in VLF CO_2 variability during LBNP. This should not be confused with static CO_2 reactivity, which appears to be maintained during LBNP, as suggested by the simultaneous drops in the steady-state values of $P_{ET_{CO_2}}$ and MCBFV (Table 1). However, the reduction in steady-state MCBFV may be also induced by the increased sympathetic activity during LBNP (53), which is evidenced by the significant increase in HR (Table 1). In this context, it is possible that modulation of sympathetic neural activity on cerebral vasomotor reactivity may be different under dynamic and steady-state conditions (48).

Study limitations. The use of CBFV as an index for CBF has been discussed extensively (24, 35, 41, 49). CBFV changes reflect CBF changes only if the cross-sectional area of the insonated vessel remains relatively constant. It has been found that the diameter of the middle cerebral artery does not change in humans during moderate LBNP (up to −40 mmHg) or changes in $P_{ET_{CO_2}}$ (41, 49). Therefore, we assumed that beat-to-beat MCBFV changes were a good index of beat-to-beat MCBF changes. The reliability of the Finapres technique for measuring changes in arterial blood pressure has also been established (19, 36). Variations of $P_{ET_{CO_2}}$ were found to be a good index of Pa_{CO_2} variations under resting conditions (45, 50). On the other hand, changes in the steady-state value of Pa_{CO_2} are possibly overestimated by the corresponding changes in $P_{ET_{CO_2}}$ under orthostatic stress, because of combined hyper-

ventilation and stroke volume reduction, which may induce a ventilation-perfusion mismatch of the lung (53), both of which may contribute to the enhanced CO_2 variability during LBNP. However, because we utilized breath-by-breath variations of $P_{ET_{CO_2}}$ around its mean value to assess cerebral vasomotor reactivity, the discrepancies that exist between steady-state values of $P_{ET_{CO_2}}$ and Pa_{CO_2} are unlikely to have affected our analysis. We speculate, though, that it might contribute to some of the discrepancies in the literature, particularly when CO_2 has been added to "normalize" $P_{ET_{CO_2}}$ (53).

It should be noted that the results of this study were obtained from spontaneous fluctuations of MABP, MCBFV, and $P_{ET_{CO_2}}$. Interpretation of these results should thus be made with caution under conditions of large changes in hemodynamic variables, even though the results obtained from the sinusoidal MABP simulations were in agreement with the experimental data. Moreover, because measurements of transient hemodynamics during or immediately before syncope (or presyncopal) were not included in the above analysis, the results shown here may not be comparable with the findings reported from experimental data before presyncope (6, 10, 46). We should also note that we selected to use two data segments (training and validation), instead of three (training, validation, and testing), owing to the relatively limited number of available data points under the induced experimental conditions. Specifically, we selected to use as many training data points as possible, while maintaining high ratios of training to validation data (320/40 = 8) and training data to model parameters (320/60 = 5.33 for the third-order models). This was also necessary for the reliable estimation of the slower dynamics of the system (kernel memory of ~80 s).

Finally, we should acknowledge the individual variability of the nonlinear Volterra kernel estimates. We speculate that this variability was due to the time-varying behavior of cerebral hemodynamics, particularly the nonlinear dynamics, which has been observed in previous studies using long-duration recordings (33, 34). Because of the subsequent variability in the location of the nonlinear frequency response spectral peaks, we assessed the effects of LBNP on the higher-order kernels by integrating their spectral power individually and group-averaging the results, instead of direct group-averaging the kernels directly in the time or frequency domains. Finally, because a third-order LVN model was selected to model cerebral hemodynamics, Volterra kernels of up to third order were estimated. In contrast to their first- and second-order counterparts, the third-order kernels cannot be easily visualized, except as multiple two-dimensional slices, making their interpretation more difficult. Thus the effects of the third-order kernels at baseline and during LBNP were assessed indirectly through the SSP of the model predictions.

In conclusion, the results obtained from a two-input, nonlinear model of cerebral hemodynamics suggest that dynamic autoregulation of the VLF MABP variations was impaired and that dynamic cerebral vasomotor reactivity was reduced under orthostatic stress. These changes may reflect a reduced cerebrovascular reserve under orthostatic stress that could result in the occurrence of large transient reductions in CBF and lead to cerebral hypoperfusion under these conditions.

REFERENCES

1. **Aaslid R, Markwalder T, and Nornes H.** Noninvasive transcranial Doppler ultrasound recording of flow velocity in basal cerebral arteries. *J Neurosurg* 57: 769–774, 1982.
2. **Aaslid R, Lindegaard KF, Sorteberg W, and Nornes H.** Cerebral autoregulation dynamics in humans. *Stroke* 20: 45–52, 1989.
3. **Blaber AP, Bondar RL, Stein F, Dunphry PT, Moradshahi P, Kassam MS, and Freeman R.** Transfer function analysis of cerebral autoregulation dynamics in autonomic failure patients. *Stroke* 28: 1686–1692, 1997.
4. **Bondar RL, Kassam MS, Stein F, Dunphy PT, Fortney S, and Riedesel ML.** Simultaneous cerebrovascular and cardiovascular responses during presyncope. *Stroke* 26: 1794–1800, 1995.
5. **Buckey JC, Lane LD, Levine BD, Watenpaugh DE, Wright SJ, Moore WE, Gaffney FA, and Blomqvist CG.** Orthostatic intolerance after spaceflight. *J Appl Physiol* 81: 7–18, 1996.
6. **Carey BJ, Manktelow BN, Panerai RB, and Potter JF.** Cerebral autoregulatory responses to head-up tilt in normal subjects and patients with recurrent vasovagal syncope. *Circulation* 104: 898–902, 2001.
7. **Chon KH, Mullen TJ, and Cohen RJ.** A dual-input nonlinear system analysis of autonomic modulation of heart rate. *IEEE Trans Biomed Eng* 43: 530–544, 1996.
8. **Chon KH, Chen YM, Holstein-Rathlou NH, and Marmarelis VZ.** Nonlinear system analysis of renal autoregulation in normotensive and hypertensive rats. *IEEE Trans Biomed Eng* 45: 342–353, 1998.
9. **Chon KH, Chen YM, Marmarelis VZ, Marsh DJ, and Holstein-Rathlou NH.** Detection of interactions between myogenic and TGF mechanisms using nonlinear analysis. *Am J Physiol Renal Fluid Electrolyte Physiol* 267: F160–F173, 1994.
10. **Dan D, Hoag JB, Ellenbogen KA, Wood MA, Eckberg DL, and Gilligan DM.** Cerebral blood flow velocity declines before arterial pressure in patients with orthostatic vasovagal presyncope. *J Am Coll Cardiol* 39: 1039–1045, 2002.
11. **Edvinsson L and Krause DN.** *Cerebral Blood Flow and Metabolism.* Philadelphia, PA: Lippincott Williams and Wilkins, 2002.
12. **Edwards MR, Shoemaker JK, and Hughson RL.** Dynamic modulation of cerebrovascular resistance as an index of autoregulation under tilt and controlled $P_{ET_{CO_2}}$. *Am J Physiol Regul Integr Comp Physiol* 283: R653–R662, 2002.
13. **Edwards MR, Topor ZL, and Hughson RL.** A new two-breath technique for extracting the cerebrovascular response to arterial carbon dioxide. *Am J Physiol Regul Integr Comp Physiol* 284: R853–R859, 2003.
14. **Ellingsen I, Hauge A, Nicolaysen G, Thoresen M, and Walloe L.** Changes in human cerebral blood flow due to step changes in Pa_{O_2} and Pa_{CO_2}. *Acta Physiol Scand* 129: 157–163, 1987.
15. **Giller CA.** The frequency-dependent behavior of cerebral autoregulation. *Neurosurgery* 27: 362–368, 1990.
16. **Grubb BP, Gerard G, Roush K, Temesy-Armos P, Montford P, Elliot L, Hahn H, and Brewster P.** Cerebral vasoconstriction during head-upright tilt-induced vasovagal syncope: a paradoxic and unexpected response. *Circulation* 84: 1157–1163, 1991.
17. **Heistad DD and Marcus ML.** Evidence that neural mechanisms do not have important effects on cerebral blood flow. *Circ Res* 42: 295–302, 1978.
18. **Heistad DD and Kontos HA.** Cerebral circulation. In: *Handbook of Physiology. The Cardiovascular System. Peripheral Circulation and Organ Blood Flow.* Bethesda, MD: Am. Physiol. Soc., 1983, sect. 2, vol. III, pt. 1, chapt. 5, p. 137–182.
19. **Imholz BP, Settels JJ, van der Meiraker AH, Wesseling KH, and Wieling W.** Non-invasive continuous finger blood pressure measurement during orthostatic stress compared with intra-arterial pressure. *Cardiovasc Res* 24: 214–221, 1990.
20. **Jian BJ, Cotter LA, Emanuel BA, Cass SP, and Yates BJ.** Effects of bilateral vestibular lesions on orthostatic tolerance in awake cats. *J Appl Physiol* 86: 1552–1560, 1999.
21. **Jordan J, Shannon JR, Diedrich A, Black B, Costa F, Robertson D, and Biaggioni I.** Interaction of carbon dioxide and sympathetic nervous system activity in the regulation of cerebral perfusion in humans. *Hypertension* 36: 383–388, 2000.
22. **Kerman IA, Emanuel BA, and Yates BJ.** Vestibular stimulation leads to distinct hemodynamic patterning. *Am J Physiol Regul Integr Comp Physiol* 279: R118–R125, 2000.

23. **Kuo TBJ, Chern CM, Sheng WY, Wong WJ, and Hu HH.** Frequency domain analysis of cerebral blood flow velocity and its correlation with arterial blood pressure. *J Cereb Blood Flow Metab* 18: 311–318, 1998.

24. **Larsen FS, Olsen KS, Hansen BA, Paulson OB, and Knudsen GM.** Transcranial Doppler is valid for determination of the lower limit of cerebral blood flow autoregulation. *Stroke* 25: 1985–1988, 1994.

25. **LeMarbre G, Stauber S, Khayat RN, Puleo DS, Skatrud JB, and Morgan BJ.** Baroreflex-induced sympathetic activation does not alter cerebrovascular CO_2 responsiveness in humans. *J Physiol* 551: 609–616, 2003.

26. **Levine BD, Buckey JC, Fritsch JM, Yancy CW Jr, Watenpaugh DE, Snell PG, Lande LD, Eckberg DL, and Blomqvist CG.** Physical fitness and cardiovascular regulation: mechanisms of orthostatic intolerance. *J Appl Physiol* 70: 112–122, 1991.

27. **Levine BD, Giller CA, Lane LD, Buckey JC, and Blomqvist CG.** Cerebral versus systemic hemodynamics during graded orthostatic stress in humans. *Circulation* 90: 298–306, 1994.

28. **Marmarelis VZ.** Coherence and apparent transfer function measurements for nonlinear physiological measurements. *Ann Biomed Eng* 16: 143–157, 1988.

29. **Marmarelis VZ.** Identification of nonlinear biological systems using Laguerre expansions of kernels. *Ann Biomed Eng* 21: 573–589, 1993.

30. **Marmarelis VZ.** *Nonlinear Dynamic Modeling of Physiological Systems.* Piscataway, NJ: IEEE-Wiley, 2004.

31. **Mitsis GD and Marmarelis VZ.** Modeling of nonlinear physiological systems with fast and slow dynamics. I. Methodology. *Ann Biomed Eng* 30: 272–281, 2002.

32. **Mitsis GD and Marmarelis VZ.** Nonlinear modeling of physiological systems with multiple inputs. *Proc 2nd Joint Meet IEEE EMBS/BMES,* Houston, TX, 2002, vol. 1, p. 21–22.

33. **Mitsis GD, Zhang R, Levine BD, and Marmarelis VZ.** Modeling of nonlinear physiological systems with fast and slow dynamics. II. Application to cerebral autoregulation. *Ann Biomed Eng* 30: 555–565, 2002.

34. **Mitsis GD, Poulin MJ, Robbins PA, and Marmarelis VZ.** Nonlinear modeling of the dynamic effects of arterial pressure and CO_2 variations on cerebral blood flow in healthy humans. *IEEE Trans Biomed Eng* 51: 1932–1943, 2004.

35. **Newell DW, Aaslid R, Lam A, Mayberg TS, and Winn HR.** Comparison of flow and velocity during dynamic autoregulation testing in humans. *Stroke* 25: 793–797, 1994.

36. **Omboni S, Parati G, Frattola A, Mutti E, Di Rienzo M, Catiglioni P, and Mancia G.** Spectral and sequence analysis of finger blood pressure variability: comparison with analysis of intra-arterial recordings. *Hypertension* 22: 26–33, 1993.

37. **Panerai RB, Kelsall AWR, Rennie JM, and Evans DH.** Frequency-domain analysis of cerebral autoregulation from spontaneous fluctuations in arterial blood pressure. *Med Biol Eng Comput* 36: 315–322, 1998.

38. **Panerai RB, Dawson SL, and Potter JF.** Linear and nonlinear analysis of human dynamic cerebral autoregulation. *Am J Physiol Heart Circ Physiol* 277: H1089–H1099, 1999.

39. **Panerai RB, Simpson DM, Deverson ST, Mahony P, Hayes P, and Evans DH.** Multivariate dynamic analysis of cerebral blood flow regulation in humans. *IEEE Trans Biomed Eng* 47: 419–421, 2000.

40. **Poulin MJ, Liang PJ, and Robbins PA.** Dynamics of the cerebral blood flow response to step changes in end-tidal P_{CO_2} and P_{O_2} in humans. *J Appl Physiol* 81: 1084–1095, 1996.

41. **Poulin MJ and Robbins PA.** Indexes of flow and cross-sectional area in the middle cerebral artery using Doppler ultrasound during hypoxia and hypercapnia in humans. *Stroke* 27: 2244–2250, 1996.

42. **Proakis JG and Manolakis DG.** *Digital Signal Processing: Principles, Algorithms, and Applications.* Upper Saddle River, NJ: Prentice-Hall, 1996.

43. **Purves MJ.** Do vasomotor nerves significantly regulate cerebral blood flow? *Circ Res* 43: 485–493, 1978.

44. **Ray CA and Monahan KD.** The vestibulosympathetic reflex in humans: neural interactions between cardiovascular reflexes. *Clin Exp Pharmacol Physiol* 29: 98–102, 2002.

45. **Robbins PA, Conway J, Cunningham DA, Khamnei S, and Patterson DJ.** A comparison of indirect methods for continuous estimation of arterial P_{CO_2} in men. *J Appl Physiol* 68: 1727–1731, 1990.

46. **Schondorf R, Benoit J, and Wein T.** Cerebrovascular and cardiovascular measurements during neurally mediated syncope induced by head-up tilt. *Stroke* 28: 1564–1568, 1997.

47. **Schondorf R, Stein R, Roberts R, Benoit J, and Cupples W.** Dynamic cerebral autoregulation is preserved in neurally mediated syncope. *J Appl Physiol* 91: 2493–2502, 2001.

48. **Sercombe R, Lacombe P, Aubineau P, Mamo H, Pinard E, Reynier-Rebuffel AM, and Seylaz J.** Is there an active mechanism limiting the influence of the sympathetic system on the cerebral vascular bed? Evidence for vasomotor escape from sympathetic stimulation in the rabbit. *Brain Res* 164: 81–102, 1979.

49. **Serrador JM, Picot PA, Rutt BK, Shoemaker JK, and Bondar RL.** MRI measures of middle cerebral artery diameter in conscious humans during simulated orthostasis. *Stroke* 31: 1672–1678, 2000.

50. **Sjöberg J.** *Non-linear System Identification With Neural Networks* (PhD thesis). Linköping, Sweden: Linköping University, 1995.

51. **Williams JS and Babb TG.** Differences between estimates and measured Pa_{CO_2} during rest and exercise in older subjects. *J Appl Physiol* 83: 312–316, 1997.

52. **Zhang R, Zuckerman JH, Giller CA, and Levine BD.** Transfer function analysis of dynamic cerebral autoregulation in humans. *Am J Physiol Heart Circ Physiol* 274: H233–H241, 1998.

53. **Zhang R, Zuckerman JH, and Levine BD.** Deterioration of cerebral autoregulation during orthostatic stress: insights from the frequency domain. *J Appl Physiol* 85: 1113–1122, 1998.

54. **Zhang R, Zuckerman JH, Iwasaki K, Wilson TE, Crandall CG, and Levine BD.** Autonomic neural control of dynamic cerebral autoregulation in humans. *Circulation* 106: 1814–1820, 2002.

55. **Zhong Y, Wang H, Ju KH, Jan KM, and Chon KH.** Nonlinear analysis of the separate contributions of autonomic nervous systems to heart rate variability using principal dynamic modes. *IEEE Trans Biomed Eng* 51: 255–262, 2004.